Antiferromagnetic NiO thickness dependent sign of the spin Hall magnetoresistance in γ –Fe_2O_3/NiO/Pt epitaxial stacks

Bo-Wen Dong,[1,2,3] Lorenzo Baldrati,[2] Christoph Schneider,[2] Tomohiko Niizeki,[4] Rafael Ramos,[4] Andrew Ross,[2,3] Joel Cramer,[2,3] Eiji Saitoh,[4,5,6,7,8] and Mathias Kläui[2,3]

[1]*School of Materials Science and Engineering, University of Science and Technology Beijing, 100083 Beijing, China*

[2]*Institute of Physics, Johannes Gutenberg-Universität Mainz, 55099 Mainz, Germany*

[3]*Graduate School of Excellence Materials Science in Mainz (MAINZ), 55128 Mainz, Germany*

[4]*Advanced Institute for Materials Research, Tohoku University, Sendai 980-8577, Japan*

[5]*Institute for Materials Research, Tohoku University, Sendai 980-8577, Japan*

[6]*Advanced Science Research Center, Japan Atomic Energy Agency, Tokai 319-1195, Japan*

[7]*Center for Spintronics Research Network, Tohoku University, Sendai 980-8577, Japan*

[8]*Department of Applied Physics, The University of Tokyo, Tokyo 113-8656, Japan*

Abstract

We study the spin Hall magnetoresistance (SMR) in epitaxial γ–Fe_2O_3/NiO(001)/Pt stacks, as a function of temperature and thickness of the antiferromagnetic insulating NiO layer. Upon increasing the thickness of the NiO from 0 nm to 10 nm, we detect a sign change of the SMR in the temperature range between 10 K and 280 K. This temperature dependence of the SMR in our stacks is different compared to that of previously studied YIG/NiO/Pt, as we do not find any peak or sign change as a function of temperature. We explain our data by a combination of spin current reflection from both the NiO/Pt and γ–Fe_2O_3/NiO interfaces and the thickness-dependent exchange coupling mode between the NiO and γ–Fe_2O_3 layers, comprising parallel alignment for thin NiO and perpendicular alignment when the NiO is thick.

In the field of spintronics, pure spin currents can transport spin angular momentum via conduction electron motion or collective propagation of magnetic moments (magnons) in absence of a charge flow.[1,2] This allows to transport information without Joule heating effects and to minimize Oersted fields, which is favorable for future applications in information technologies.[3] The prototypical systems for the study of pure spin currents are ferromagnetic insulator (FMI)/heavy metal (HM) heterostructures, where spin currents can be generated by the spin Seebeck effect (SSE)[4-6] or spin pumping (SP).[7,8] In addition to this, in HM layers with a large spin-orbit coupling, a longitudinal charge current can induce a transverse spin current, with polarization $\boldsymbol{\sigma}$, via the spin Hall effect (SHE).[9] This is at the origin of the so-called spin Hall magnetoresistance (SMR): the spin current travels across the FMI/HM interface, injecting spin angular momentum into the FMI.[10] When the magnetization of the FMI and induced spin accumulation in HM are parallel, the spin current is reflected back into the HM layer and re-converted to a charge current via the inverse SHE (ISHE).[11] The rotation of the normalized magnetization ($\boldsymbol{m}_{\mathbf{FM}}$) in the FMI layer modulates the absorption/reflection of the spin current via spin transfer torque, leading to a measurable resistance change in the HM.

So far, the SMR has been intensively studied in both collinear[12] and non-collinear[13-15] FMI and, more recently, in antiferromagnetic insulators (AFMIs) where the normalized Néel vector ($\boldsymbol{n}_{\mathbf{AFM}}$) plays the same role as $\boldsymbol{m}_{\mathbf{FM}}$.[16-21] Antiferromagnets entail advantages over ferromagnets, including ultrafast dynamics in the THz range and robustness against external magnetic fields.[22] However, the manipulation of $\boldsymbol{n}_{\mathbf{AFM}}$ in stand-alone AFMIs often requires large fields, which are difficult to generate and not suitable for applications, and also implying that intrinsic effects from the HM such as ordinary magnetoresistance (OMR) and Hanle magnetoresistance (HMR)[23] may obscure the SMR signal. One possibility to avoid this is to employ ferromagnetic layers to control the $\boldsymbol{n}_{\mathbf{AFM}}$ via exchange coupling between the AFMI and FMI. In FMI/AFMI/HM stacks, a thin AFMI layer has been shown to transmit spin angular momentum between a FMI, where a spin current is generated by the SSE or SP, to a HM

layer, where the spin current is detected by the ISHE.[24-27] On the other hand, a sign change of the SMR signal has been observed in YIG (yttrium iron garnet, $Y_3Fe_5O_{12}$)/NiO/Pt stacks, in which YIG is a widely-used FMI due to its large band gap, low damping and small saturation field and NiO is a typical insulating easy-plane antiferromagnet.[28-30] However, the origin of the sign change is debated: Hou *et al.*[29] attribute the negative SMR to the Néel order of the NiO that is spin flop coupled to the YIG, as recently supported by polarized neutron reflectometry,[31] while Lin *et al.*[30] propose that the mechanism relies on the spin-flip scattering for the spin current flowing back from the exchange coupled YIG/NiO interface to the Pt. Another work on YIG/NiO/Pt found no sign change of the SMR as a function of the NiO thickness.[32] However, in previous SMR studies, the NiO was polycrystalline. This makes the comparison of the results rather tenuous, because the different behaviors might stem from different NiO properties (crystallite sizes, orientations, etc.). In contrast to this, epitaxial stacks allow for well-defined material properties and a clear crystalline structure with little disorder.

In this manuscript, we study the temperature and NiO thickness dependence of the SMR in heterostructures comprising epitaxial maghemite (γ-Fe_2O_3)/NiO/Pt stacks. γ-Fe_2O_3 is a FMI with an inverse spinel crystal structure of a lattice constant $a_{\gamma-Fe2O3}$ = 8.34 Å, enabling the epitaxial growth of NiO, which has a rock salt structure and a lattice constant of a_{NiO} = 4.18 Å.[33] Previous reports revealed that iron oxides, including γ-Fe_2O_3 and magnetite (Fe_3O_4), are efficient thermal spin current generators,[34-36] but the SMR in these materials has been rarely reported.[37] Here, we analyze the magnitude and angular dependence of the SMR in γ-Fe_2O_3/Pt and compare to the case with an epitaxial antiferromagnetic NiO insert layer with variable thickness and at different temperatures. While the temperature dependence of the SMR does not show any sign change, in contrast to what was reported in YIG/NiO/Pt,[29,30] we find that the NiO thickness dependence non-trivially reveals a sign change, entailing a complex exchange coupling between γ-Fe_2O_3 and NiO, favoring parallel alignment at low NiO thickness and perpendicular alignment at high NiO thickness.

Epitaxial γ-Fe_2O_3/NiO stacks were grown by radio frequency (RF) magnetron sputtering in a mixed Ar/O_2 atmosphere on MgO(001) substrates with a 6 nm NiO buffer layer. The epitaxial growth of the stacks was checked via x-ray diffraction (XRD). The blue and red curve in Fig. 1(a) show the ω/2θ XRD scans for γ-Fe_2O_3/NiO (10 nm) and γ-Fe_2O_3/NiO (5 nm) stacks, respectively. The γ-Fe_2O_3 (004) peak is found in both samples at $2\theta \approx 43.72°$ and the clear Laue oscillations indicate high uniformity and crystallinity throughout the film. Further details on the growth conditions and epitaxial quality of NiO can be found elsewhere.[27] To ensure comparable interface conditions and maximize uniformity of the samples for the SMR study, we deposited NiO with different thickness steps by means of an *in-situ* linear shutter on top of a uniform 40 nm thick γ-Fe_2O_3 layer (Fig. 1(b)). Subsequently, a 3.5 nm thick Pt layer was deposited by DC sputtering at room temperature without breaking the vacuum. The samples were cut into pieces with the following different NiO thicknesses t_{NiO} = 0, 1, 3, 5, 7, 10 nm and then they were measured.

To study the SMR, we performed angular dependent magnetoresistance measurements (ADMR) in a helium cooled 3D vector cryostat. By rotating the magnetization $\mathbf{M}$ of the γ-Fe_2O_3 layer with a magnetic field of fixed magnitude (0.8 T) in the xy, xz and yz planes defined in Fig. 2(a), we measure the variation of the longitudinal resistance of the Pt. The charge current $\mathbf{J}_c$ applied along the x axis generates a spin current with polarization $\boldsymbol{\sigma}$ parallel to the y axis by the SHE in Pt, and therefore a non-equilibrium spin accumulation builds up at the interfaces of NiO/Pt or γ-Fe_2O_3/NiO, if the spin current is transmitted through the NiO layer. At the interfaces, the ferromagnetic magnetic moment $\boldsymbol{m_{FM}}$ or the antiferromagnetic Néel vector $\boldsymbol{n_{AFM}}$ can either absorb the spin current, when $\boldsymbol{m_{FM}}(\boldsymbol{n_{AFM}}) \perp \boldsymbol{\sigma}$, or reflect it when $\boldsymbol{m_{FM}}(\boldsymbol{n_{AFM}}) \parallel \boldsymbol{\sigma}$.[12,17] The reflected spin currents are re-converted into a longitudinal charge current by the ISHE, and thus the measured resistivity $\boldsymbol{\rho}$ of the Pt depends on the angle θ between $\boldsymbol{m_{FM}}(\boldsymbol{n_{AFM}})$ and $\boldsymbol{\sigma}$, following the relation $\boldsymbol{\rho} = \boldsymbol{\rho_0} + \Delta\boldsymbol{\rho}\boldsymbol{m_y^2} = \boldsymbol{\rho_0} + \Delta\boldsymbol{\rho}\sin^2\theta$, where $\boldsymbol{\rho_0}$ is the magnetization independent electric resistivity of the Pt, $\Delta\boldsymbol{\rho}$ is the change of resistivity due to the SMR

and $\boldsymbol{m_y}$ is the component of the normalized magnetization in the y-direction. The SMR depends on the angle between $\mathbf{M}$ and $\boldsymbol{\sigma}$, in contrast to the AMR which depends on the angle between $\mathbf{M}$ and $\mathbf{J}_c$, so that the two can be distinguished by ADMR measurements.

Figure 2(b) and (c) show the ADMR results in a γ-Fe_2O_3/Pt sample with external field $\left|\mu_0 \boldsymbol{H}\right| = 0.8$ T at 250 K and 10 K in three orthogonal planes, respectively. One can clearly see that, at both temperatures, the MR exhibits a similar angular dependence and no visible MR appears when the external field rotates in the xz plane (γ-scan), showing that there is no significant AMR contribution from possible magnetic proximity effects (MPE) in Pt.[38] We can thus exclude the MPE in γ-Fe_2O_3/Pt even at low temperatures, which corroborates the reliability of spin pumping and SSE results in related structures in this temperature range.[27] By rotating the field in the xy plane (α-scan) and yz plane (β-scan), we have magnetoresistance variations dominated by the SMR, where the angular dependence follows the relation mentioned above as $\alpha = 90° - \theta$ and $\beta = \theta$. Note that the β-scan SMR shows some deviations from $\sin^2\beta$ due to the non-collinearity between H and M induced by the easy in-plane magnetic anisotropy during the out of plane rotation of the external field, that is not large enough to completely saturate the magnetization along the field for all directions. We calculated the SMR ratio

$$\text{SMR ratio} = \frac{R(\beta=90^\circ) - R(\beta=180^\circ)}{R(\beta=180^\circ)}, \quad (1)$$

obtaining a value of 3.8×10^{-4} at 250 K. According to the spin-diffusion theory in FMI/HM, the SMR ratio depends on the real part of the interfacial spin-mixing conductance G_r as

$$\text{SMR ratio} = \theta_{SH}^2 \frac{\lambda^2}{t} \frac{2G_r \tanh^2\frac{t}{2\lambda}}{\sigma + 2\lambda G_r \coth\frac{t}{\lambda}}, \quad (2)$$

in which θ_{SH}, λ, t, σ are the spin Hall angle, spin diffusion length, thickness and electrical conductivity of HM, respectively.[39] Therefore, the effective G_r in the γ-Fe_2O_3/Pt estimated via Eq. (2) using $\theta_{SH} \sim 0.068$ and $\lambda \sim 1.5$ nm[40] is $1.3 \times 10^{14}\ \Omega^{-1}m^{-1}$, and thus of the same order of magnitude as previously found for YIG/Pt heterstructures.[41]

Having established the suitability of γ-Fe_2O_3 for SMR, we next consider the effect of inserting a NiO layer in the stack. Figure 3 shows the isothermal NiO thickness dependence of the SMR measured by ADMR measurements at 280 K. Note that we used a relatively small field of $|\mu_0 \boldsymbol{H}|$ = 0.8 T, which allows us to exclude Hanle and ordinary magnetoresistance in the Pt.[23] One can see that when a thin NiO layer (1 nm, 3 nm, 5 nm) is inserted, the positive SMR ratio decreases and vanishes when the NiO layer is 7 nm thick. Importantly, the SMR signal emerges again with negative sign when the NiO is 10 nm thick. The fact that the SMR signal does not decay exponentially to zero, demonstrates that the NiO plays an active role in governing the SMR signal, and is not a mere attenuator of the spin current. For γ-Fe_2O_3/Pt, without NiO, the β-scan ADMR shows positive SMR sign, i.e. the resistance of Pt is smaller when H $\left(\boldsymbol{m}_{\gamma-Fe_2O_3}\right) \parallel \boldsymbol{y}(\boldsymbol{\sigma})$ compared to H $\left(\boldsymbol{m}_{\gamma-Fe_2O_3}\right) \perp \boldsymbol{y}(\boldsymbol{\sigma})$. The SMR exhibits an opposite sign for a NiO thickness larger than 7 nm. In contrast to previous reports in YIG/NiO/Pt trilayers,[29,30] we can exclude that the negative SMR stems from the spin flip reflection at the γ-Fe_2O_3/NiO interface,[30] since the SMR sign change occurs at a NiO thickness of 7 nm, where the transmission of spin current is significantly suppressed in NiO on this length scale[27]. The negative sign of the SMR at 10 nm of NiO thickness was confirmed also by ADMR α-scans.

In general, the spin currents generated in the Pt layer are partly reflected by the NiO Néel vector at the NiO/Pt interface and partly penetrate through the NiO towards the γ-Fe_2O_3/NiO bottom interface,[26] where they are once again partly reflected. So in general the measured signal is a superposition of both signals. We find thus that the bottom γ-Fe_2O_3/NiO interface plays the dominant role only when the NiO layer is thin, as can be seen by the similar magnitude and temperature dependence (as shown below) of the SMR between the samples with 0 and 1 nm of the NiO. The increase of the NiO layer thickness t_{NiO} has two consequences: first the larger absorption of the spin current in the NiO prevents the spins from reaching the γ-Fe_2O_3 layer, and second the antiferromagnetic Néel order gives rise to a SMR at the NiO/Pt interface. Eventually at t_{NiO} = 10 nm, the negative SMR indicates a

main contribution from the NiO/Pt interface and a 90° angle between the NiO Néel vector and the external field ($\beta = 90° - \theta$). We recently reported a negative SMR in epitaxial antiferromagnetic NiO(001)/Pt bilayers without any ferromagnetic layer, resulting from the preferential perpendicular orientation of the Néel vector with respect to the external magnetic field, which induces a redistribution of the antiferromagnetic domains.[21] However, large fields (of the order of 10 T) were needed to induce a significant and clearly visible SMR.[18,21] Therefore the sizable negative SMR that we find here can be attributed to the modulation of the NiO Néel order via the spin flop exchange coupling between the NiO and γ-Fe_2O_3 layer. This leads to a perpendicular alignment of the NiO Néel order and magnetization of γ-Fe_2O_3, which in turn is parallel to the external field ($H \parallel \boldsymbol{m}_{\gamma-Fe2O3} \perp \boldsymbol{n}_{NiO}$).[29,31] The total SMR ratio is thus determined by the interfacial conditions (e.g. spin mixing conductance) and the spin transparency of the AFMI NiO layer.

To further investigate the different contributions, we measured the temperature dependence of the SMR ratio, shown in Fig. 4. In the γ-Fe_2O_3/Pt sample, the SMR decreases monotonically with temperature, which can be in general affected by the three spin transport parameters θ_{SH}, λ, G_r (see Eq. (2)) of Pt. However, simplified models have been proposed, where the temperature dependence of the SMR in YIG/Pt mainly results from changes of the spin diffusion length (λ) of Pt[41] or by a decrease of the spin Hall angle (θ_{SH}) of Pt at low temperatures[42]. We find that our data can be described by a monotonic temperature dependence of θ_{SH} in Pt for fixed other parameters. However, the clarification of this point is beyond the scope of our present work and should be addressed by future studies. By inserting the NiO layers, the amplitude of the SMR changes, but the temperature dependence maintains a similar behavior. The SMR ratio in each sample does not change its sign for the whole temperature range except for the sample comprising a 7 nm thick NiO layer, where a SMR is not detectable even at low temperatures. This behavior exhibits distinct differences compared to the one previously reported in YIG/NiO/Pt systems, where, due to the paramagnetic - antiferromagnetic transition of the NiO layer at T_N, the

SMR in the samples that have positive SMR at high temperatures shows a sign change at low temperatures.[29,30] Note that, in the presence of an inserted NiO layer, the spin transparency of the AFMI NiO layer also depends on the temperature, and was reported both theoretically[43] and experimentally[26,29] to be nearly zero for the low temperature limit and peak at the Néel temperature (T_N). However, for thin epitaxial NiO films, T_N can be significantly higher than that of polycrystalline films, so that the Néel ordering temperature is expected to be outside our studied temperature range. For instance Alders *et al.*[44] found a Néel temperature of 295 K on a ~ 1 nm thick NiO(001) thin film on a MgO(001) substrate. Note that we recently observed a monotonic temperature dependence for the SSE signal in the same epitaxial γ-Fe_2O_3/NiO thin films,[27] where we found that the Néel temperature was outside of the studied temperature range. Taken together, our SSE and SMR data suggest that the Néel temperature of epitaxial NiO thin films is much higher than that of polycrystalline films.

We next consider that the SMR in γ-Fe_2O_3/NiO/Pt are positive throughout the measurement temperature range when t_{NiO} = 1, 3, 5 nm. Given that the transmission of spin in NiO is nearly zero for the low temperature limit,[26,29,43] this can be explained by considering that in samples with thin NiO (i.e. 1 nm, 3 nm and 5 nm) at low temperatures the exchange coupling alignment mode between the NiO Néel vector and the γ-Fe_2O_3 magnetization is parallel. Note that, as discussed above, the negative SMR found in the 10 nm NiO sample indicates perpendicular alignment between the NiO Néel vector with respect to the magnetic moments of the γ-Fe_2O_3, which are always aligned by the external fields. Therefore, our results indicate a transition in the exchange coupling between the antiferromagnetic (AFM) NiO and the ferrimagnetic (FM) γ-Fe_2O_3, from parallel at low NiO thickness to perpendicular at high thickness. Both collinear and perpendicular coupling between the AFM Néel order and the magnetization were directly imaged in exchanged coupled AFM/FM systems, by the synchrotron based x-ray magnetic circular/linear dichroism technique.[45-49] Controversial findings on the transition between the two coupling modes when varying the thickness of the AFM layer have been reported: M. Finazzi *et al.*[46] found that

the NiO magnetic anisotropy axis of a NiO/Fe film rotates from perpendicular to parallel to the magnetization of the bottom Fe layer when increasing the NiO film thickness, while J. Wu *et al.*[47] found an opposite behavior in similar systems. For γ-Fe_2O_3/NiO(001) epitaxial stacks, we find that the collinear to perpendicular coupling transition occurs by increasing the NiO thickness, in agreement with what was reported in NiO/Fe.[47] The NiO thickness dependence of the SMR at low temperatures therefore indicates possibly a continuous transition from parallel to perpendicular coupling between γ-Fe_2O_3 and NiO. The vanishing SMR in the 7 nm NiO sample can be then attributed to a multi-domain state of the NiO layer, where collinear and perpendicular domains are similarly numerous in the sample and their overall net contribution to SMR superposes to a small value below the detection limit of the measurement.[15]

In summary, we investigated SMR in epitaxial stacks consisting of γ-Fe_2O_3/NiO(001)/Pt with varying thickness of the NiO layer. We observed a sign change of the SMR when the thickness of the NiO layer is increased. The temperature dependence of the SMR ratio in all samples is monotonic and no sign change is observed as a function of temperature, in contrast to what has been reported in the YIG/NiO/Pt system, where the NiO layer used is polycrystalline. The SMR behavior we found in γ-Fe_2O_3/NiO(001)/Pt trilayers, however, can be explained by a thickness dependent transition of the exchange coupling mode between γ-Fe_2O_3 and NiO, as previously observed in NiO/Fe: parallel alignment in the case of a thin NiO layer (<7 nm) and a perpendicular alignment when the NiO is thick (>7 nm). Our results show that the SMR can provide useful information to study transitions of the antiferromagnetic exchange coupling in AFM/FM bilayers and highlight the importance of the study of spin transport in well-defined epitaxial hybrid structures, whose behavior can be significantly different compared to the one of systems including polycrystalline layers.

Acknowledgements

This work was supported by Deutsche Forschungsgemeinschaft (DFG) Grant No. SPP 1538 “Spin Caloric

Transport," the Graduate School of Excellence Materials Science in Mainz (MAINZ), and the EU project INSPIN (Project No. FP7-ICT-2013-X 612759). The authors acknowledge the support of SpinNet (DAAD Spintronics network, Project No. 56268455), MaHoJeRo (DAAD Spintronics network, Project No. 57334897), and the DFG (Grant No. SFB TRR 173 SPIN+X). This work was supported by ERATO "Spin Quantum Rectification Project" (Grant No. JPMJER1402) from JST, Japan; Grant-in-Aid for Scientific Research on Innovative Area, "Nano Spin Conversion Science" (Grant No. JP26103005) from JSPS KAKENHI, Japan, and the NEC Corporation. M.K. thanks ICC-IMR at Tohoku University for their hospitality during a visiting researcher stay at the Institute for Materials Research. L. B. acknowledges funding from the European Union's Horizon 2020 research and innovation programme under the Marie Skłodowska-Curie grant agreement ARTES No 793159.

[1] S. Maekawa, S. O. Valenzuela, E. Saitoh, and A. Kimura, *Spin current* (Oxford University Press, Oxford, 2012).

[2] Y. Kajiwara, K. Harii, S. Takahashi, J. Ohe, K. Uchida, M. Mizuguchi, H. Umezawa, H. Kawai, K. Ando, K. Takanashi, S. Maekawa, and E. Saitoh, Nature **464**, 262 (2010).

[3] S. Maekawa, *Concepts in Spin Electronics* (Oxford University Press, 2012).

[4] K. Uchida, J. Xiao, H. Adachi, J. Ohe, S. Takahashi, J. Ieda, T. Ota, Y. Kajiwara, H. Umezawa, H. Kawai, G. E. W. Bauer, S. Maekawa, and E. Saitoh, Nat. Mater. **9**, 894 (2010).

[5] J. Cramer, E. J. Guo, S. Geprags, A. Kehlberger, Y. P. Ivanov, K. Ganzhorn, F. Della Coletta, M. Althammer, H. Huebl, R. Gross, J. Kosel, M. Klaui, and S. T. B. Goennenwein, Nano Lett. **17**, 3334 (2017).

[6] G. E. W. Bauer, E. Saitoh, and B. J. van Wees, Nat. Mater. **11**, 391 (2012).

[7] B. Heinrich, C. Burrowes, E. Montoya, B. Kardasz, E. Girt, Y.-Y. Song, Y. Sun, and M. Wu, Phys. Rev. Lett. **107**, 066604 (2011).

[8] Y. Sun, H. Chang, M. Kabatek, Y.-Y. Song, Z. Wang, M. Jantz, W. Schneider, M. Wu, E. Montoya, B. Kardasz, B. Heinrich, S. G. E. te Velthuis, H. Schultheiss, and A. Hoffmann, Phys. Rev. Lett. **111**, 106601 (2013).

[9] J. Sinova, S. O. Valenzuela, J. Wunderlich, C. H. Back, and T. Jungwirth, Rev. Mod. Phys. **87**, 1213 (2015).

[10] L. J. Cornelissen, J. Liu, R. A. Duine, J. B. Youssef, and B. J. van Wees, Nat. Phys. **11**, 1022 (2015).

[11] E. Saitoh, M. Ueda, H. Miyajima, and G. Tatara, Appl. Phys. Lett. **88**, 182509 (2006).

[12] H. Nakayama, M. Althammer, Y.-T. Chen, K. Uchida, Y. Kajiwara, D. Kikuchi, T. Ohtani, S. Geprägs, M. Opel, S. Takahashi, R. Gross, G. E. W. Bauer, S. T. B. Goennenwein, and E. Saitoh, Phys. Rev. Lett. **110**, 206601 (2013).

[13] A. Aqeel, N. Vlietstra, A. Roy, M. Mostovoy, B. J. van Wees, and T. T. M. Palstra, Phys. Rev. B **94**, 134418 (2016).

[14] K. Ganzhorn, J. Barker, R. Schlitz, B. A. Piot, K. Ollefs, F. Guillou, F. Wilhelm, A. Rogalev, M. Opel, M. Althammer, S. Geprägs, H. Huebl, R. Gross, G. E. W. Bauer, and S. T. B. Goennenwein, Phys. Rev. B **94**, 094401 (2016).

[15] B.-W. Dong, J. Cramer, K. Ganzhorn, Y. H. Y., G. Er-Jia, S. T. B. Goennenwein, and M. Kläui, J. Phys.: Condens. Matter **30**, 035802 (2018).

[16] J. H. Han, C. Song, F. Li, Y. Y. Wang, G. Y. Wang, Q. H. Yang, and F. Pan, Phys. Rev. B **90**, 144431 (2014).

[17] A. Manchon, physica status solidi (RRL) – Rapid Research Letters **11**, 1600409, 1600409 (2017).

[18] G. R. Hoogeboom, A. Aqeel, T. Kuschel, T. T. M. Palstra, and B. J. van Wees, Appl. Phys. Lett. **111**, 052409 (2017).

[19] J. Fischer, O. Gomonay, R. Schlitz, K. Ganzhorn, N. Vlietstra, M. Althammer, H. Huebl, M. Opel, R. Gross, S. T. B. Goennenwein, and S. Geprägs, Phys. Rev. B **97**, 014417 (2018).

[20] R. Lebrun, A. Ross, S. A. Bender, A. Qaiumzadeh, L. Baldrati, J. Cramer, A. Brataas, R. A. Duine, and M. Kläui, Nature **561**, 222 (2018).

[21] L. Baldrati, A. Ross, T. Niizeki, C. Schneider, R. Ramos, J. Cramer, O. Gomonay, M. Filianina, T. Savchenko, D. Heinze, A. Kleibert, E. Saitoh, J. Sinova, and M. Kläui, Phys. Rev. B **98**, 024422 (2018).

[22] V. Baltz, A. Manchon, M. Tsoi, T. Moriyama, T. Ono, and Y. Tserkovnyak, Rev. Mod. Phys. **90**, 015005 (2018).

[23] S. Vélez, V. N. Golovach, A. Bedoya-Pinto, M. Isasa, E. Sagasta, M. Abadia, C. Rogero, L. E. Hueso, F.

S. Bergeret, and F. Casanova, Phys. Rev. Lett. **116**, 016603 (2016).
[24] H. L. Wang, C. H. Du, P. C. Hammel, and F. Y. Yang, Phys. Rev. Lett. **113**, 097202 (2014).
[25] W. Lin, K. Chen, S. Zhang, and C. L. Chien, Phys. Rev. Lett. **116**, 186601 (2016).
[26] Z. Qiu, J. Li, D. Hou, E. Arenholz, A. T. N'Diaye, A. Tan, K. Uchida, K. Sato, S. Okamoto, Y. Tserkovnyak, Z. Q. Qiu, and E. Saitoh, Nat. Commun. **7**, 12670 (2016).
[27] L. Baldrati, C. Schneider, T. Niizeki, R. Ramos, J. Cramer, A. Ross, E. Saitoh, and M. Kläui, Phys. Rev. B **98**, 014409 (2018).
[28] T. Shang, Q. F. Zhan, H. L. Yang, Z. H. Zuo, Y. L. Xie, L. P. Liu, S. L. Zhang, Y. Zhang, H. H. Li, B. M. Wang, Y. H. Wu, S. Zhang, and R.-W. Li, Appl. Phys. Lett. **109**, 032410 (2016).
[29] D. Hou, Z. Qiu, J. Barker, K. Sato, K. Yamamoto, S. Vélez, J. M. Gomez-Perez, L. E. Hueso, F. Casanova, and E. Saitoh, Phys. Rev. Lett. **118**, 147202 (2017).
[30] W. Lin and C. L. Chien, Phys. Rev. Lett. **118**, 067202 (2017).
[31] Z. Z. Luan, F. F. Chang, P. Wang, L. F. Zhou, J. F. K. Cooper, C. J. Kinane, S. Langridge, J. W. Cai, J. Du, T. Zhu, and D. Wu, Appl. Phys. Lett. **113**, 072406 (2018).
[32] Y.-M. Hung, C. Hahn, H. Chang, M. Wu, H. Ohldag, and A. D. Kent, AIP Advances **7**, 055903 (2016).
[33] J. M. D. Coey, *Magnetism and Magnetic Materials* (Cambridge Univ. Press, New York, 2010).
[34] A. Anadón, R. Ramos, I. Lucas, P. A. Algarabel, L. Morellón, M. R. Ibarra, and M. H. Aguirre, Appl. Phys. Lett. **109**, 012404 (2016).
[35] P. Jiménez-Cavero, I. Lucas, A. Anadón, R. Ramos, T. Niizeki, M. H. Aguirre, P. A. Algarabel, K. Uchida, M. R. Ibarra, E. Saitoh, and L. Morellón, APL Materials **5**, 026103 (2017).
[36] R. Ramos, T. Kikkawa, M. H. Aguirre, I. Lucas, A. Anadón, T. Oyake, K. Uchida, H. Adachi, J. Shiomi, P. A. Algarabel, L. Morellón, S. Maekawa, E. Saitoh, and M. R. Ibarra, Phys. Rev. B **92**, 220407 (2015).
[37] Z. Ding, B. L. Chen, J. H. Liang, J. Zhu, J. X. Li, and Y. Z. Wu, Phys. Rev. B **90**, 134424 (2014).
[38] S. Y. Huang, X. Fan, D. Qu, Y. P. Chen, W. G. Wang, J. Wu, T. Y. Chen, J. Q. Xiao, and C. L. Chien, Phys. Rev. Lett. **109**, 107204 (2012).
[39] Y.-T. Chen, S. Takahashi, H. Nakayama, M. Althammer, S. T. B. Goennenwein, E. Saitoh, and G. E. W. Bauer, Phys. Rev. B **87**, 144411 (2013).
[40] M. Althammer, S. Meyer, H. Nakayama, M. Schreier, S. Altmannshofer, M. Weiler, H. Huebl, S. Geprägs, M. Opel, R. Gross, D. Meier, C. Klewe, T. Kuschel, J.-M. Schmalhorst, G. Reiss, L. Shen, A. Gupta, Y.-T. Chen, G. E. W. Bauer, E. Saitoh, and S. T. B. Goennenwein, Phys. Rev. B **87**, 224401 (2013).
[41] S. R. Marmion, M. Ali, M. McLaren, D. A. Williams, and B. J. Hickey, Phys. Rev. B **89**, 220404 (2014).
[42] S. Meyer, M. Althammer, S. Geprägs, M. Opel, R. Gross, and S. T. B. Goennenwein, Appl. Phys. Lett. **104**, 242411 (2014).
[43] S. Okamoto, Phys. Rev. B **93**, 064421 (2016).
[44] D. Alders, L. H. Tjeng, F. C. Voogt, T. Hibma, G. A. Sawatzky, C. T. Chen, J. Vogel, M. Sacchi, and S. Iacobucci, Phys. Rev. B **57**, 11623 (1998).
[45] M. Finazzi, M. Portalupi, A. Brambilla, L. Duò, G. Ghiringhelli, F. Parmigiani, M. Zacchigna, M. Zangrando, and F. Ciccacci, Phys. Rev. B **69**, 014410 (2004).
[46] M. Finazzi, A. Brambilla, P. Biagioni, J. Graf, G. H. Gweon, A. Scholl, A. Lanzara, and L. Duò, Phys. Rev. Lett. **97**, 097202 (2006).
[47] J. Wu, D. Carlton, J. S. Park, Y. Meng, E. Arenholz, A. Doran, A. T. Young, A. Scholl, C. Hwang, H. W. Zhao, J. Bokor, and Z. Q. Qiu, Nat. Phys. **7**, 303 (2011).
[48] H. Ohldag, A. Scholl, F. Nolting, S. Anders, F. U. Hillebrecht, and J. Stöhr, Phys. Rev. Lett. **86**, 2878 (2001).

[49] H. Ohldag, T. J. Regan, J. Stöhr, A. Scholl, F. Nolting, J. Lüning, C. Stamm, S. Anders, and R. L. White, Phys. Rev. Lett. **87**, 247201 (2001).

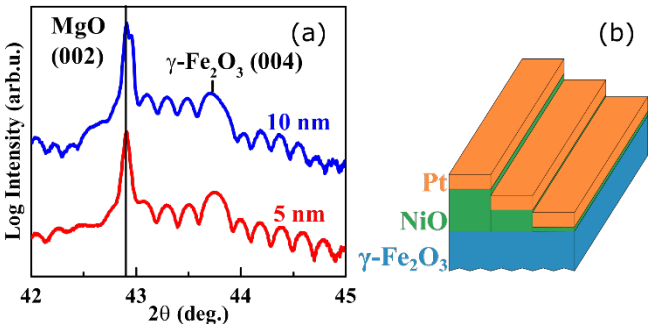

FIG.1 (a) XRD data of MgO//NiO(6 nm)/γ-Fe_2O_3(40 nm)/NiO(5 nm)/Pt (red line) and MgO//NiO(6 nm)/γ-Fe_2O_3(40 nm)/NiO(10 nm)/Pt (blue line). (b) Schematic of the film stacks of γ-Fe_2O_3/NiO/Pt with NiO thickness steps of 1 nm, 5 nm and 10 nm.

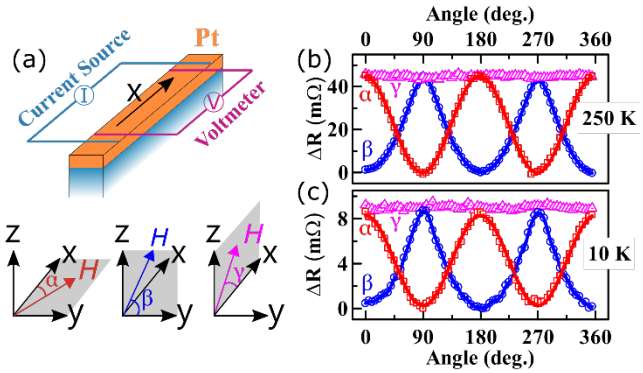

FIG. 2 (a) Scheme of the angular dependent magnetoresistance (ADMR) measurement. The magnetic field H is applied in the xy, yz, and zx planes with angles α, β, and γ relative to the x, z, and x directions, respectively. The current is applied along the x axis in all measurements. (b) and (c) ADMR results in γ-Fe_2O_3/Pt under an external field of 0.8 T at 250 K (b) and 10 K (c), respectively.

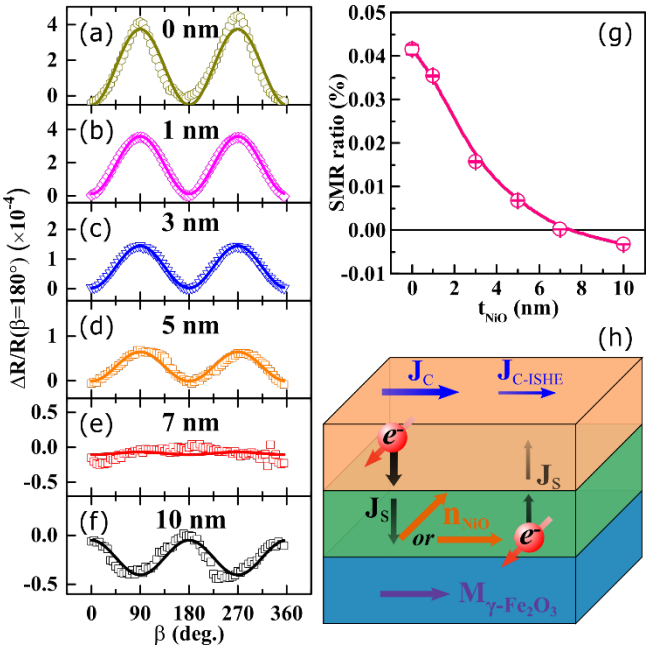

FIG. 3 (a) - (f) ADMR measurements with an external field $|\mu_0 \boldsymbol{H}|$ = 0.8 T rotated within the yz plane (β scan) at 280 K for γ-Fe_2O_3(40 nm)/NiO(t_{NiO})/Pt with different NiO thickness (t_{NiO} = 0, 1, 3, 5, 7, 10 nm). $\Delta R = R(\beta = 90^{\circ}) - R(\beta = 180^{\circ})$. (g) SMR ratio as a function of the NiO layer thickness t_{NiO} measured at 280 K and external field of 0.8 T. The line is a guide to the eye. (h) Schematic of spin reflection at NiO/Pt and γ-Fe_2O_3/NiO interfaces and spin transmission in the AFMI NiO.

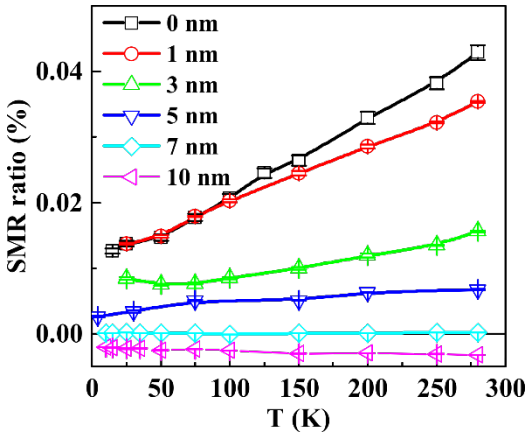

FIG. 4 SMR ratio measured in γ-Fe_2O_3(40 nm)/NiO(t_{NiO})/Pt with different NiO thickness (t_{NiO} = 0, 1, 3, 5, 7, 10 nm) as a function of temperature.